Journal of Hydraulic Structures
J. Hydraul. Struct., 2023; 9(1):98-110
DOI: 10.22055/jhs.2023.43960.1256

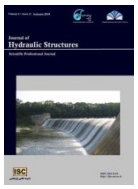

OPEN ACCESS

Discharge coefficient of combined rectangular-triangular weirs using soft computing models

Hamidreza Abbaszadeh [1]
Reza Norouzi [2]
Veli Sume [3]
Rasoul Daneshfaraz[4]
Reza Tarinejad[1]

Abstract

This study investigates the potential of Adaptive Neuro-fuzzy inference system (ANFIS), M5P, and Gaussian Process regression (GP) approaches to predict discharge coefficient (C_d) of chimney weir with different apex angles. Out of 110 data points, 77 arbitrarily selected observations were used for training, whereas the remaining 77 data points were used for testing. Input data consisted of h/p, y/p, L/p, and w/z, whereas C_d was an output. Four shapes of membership functions, i.e., triangular, trapezoidal, generalized bell-shaped, and Gaussian, were used for the ANFIS-based model development. Five different goodness-of-fit parameters and various graphical presentations were used to evaluate the performance of the machine-learning models. It was found that the M5P-based model was superior to other implemented models in predicting the C_d with Correlation Coefficient (CC) (0.9532 and 0.9472), Mean Absolute Error (MAE) (0.0024 and 0.0026), (Root Mean Square Error) RMSE (0.0032 and 0.0033), Scattering Index (SI) (0.0048 and 0.0050), and Nash Sutcliffe Efficiency (NSE) (0.9085 and 0.9925) values in the training and testing stages, respectively. Another major outcome of this study was that the ANFIS model was better than GP and other MFs-based ANFIS-ti models. The sensitivity of the C_d variables is also investigated, which showed h/p and L/p as major influencing factors in the C_d.

Keywords: discharge coefficient, chimney weir, soft computing, ANFIS, GP, M5P.

Received: 09 June 2023; Accepted: 26 June 2023

[1] Department of Water Engineering, Faculty of Civil Engineering, University of Tabriz, Tabriz, Iran.
[2] Department of Civil Engineering, Faculty of Engineering, University of Maragheh, Maragheh, Iran.
[3] Department of Civil Engineering, Faculty of Engineering, Recep Tayyip Erdogan University, Rize, Turkey.
[4] Department of Civil Engineering, Faculty of Engineering, University of Maragheh, Maragheh, Iran. E-mail: daneshfaraz@maragheh.ac.ir **(Corresponding author)**

1. Introduction

In irrigation networks, measuring the amount of water delivered is particularly important. Researchers are trying to select structures with higher performance and more effective exploitation. There are various methods for measuring water inflow into the networks and controlling water level, the most common and widely used are weirs. Proportional linear weirs are a type of weir in which the water head changes proportion to the discharge. Due to a linear relationship between the water head and discharge in linear proportional weirs, the error in reading the water head is reflected linearly in the discharge. For other weirs, there can be a greater error. Therefore, finding the optimal shape is important. Different forms of proportional weirs have been studied by different researchers with the development of relationships and equations. Stout first proposed the original idea for proportional weirs. However, his attempt to build a cross-section that facilitated the measurement of the water head was unsuccessful due to the infinite width of the weir crest [1]. To solve this problem, Sutro developed the Sutro weirs by placing a linear proportional weir on a rectangular weir [2].

Ramamurthy et al. [3] investigated the weir with a quadratic cross-section on rectangular, triangular, and circular sections. They examined the C_d and reported a linear relationship between discharge and head. Keshava Murthy and Giridhar [4] considered an inverted triangular weir and obtained a theoretical relationship for this type of weir. They examined the experimental performance of an inverted triangular weir with various vertex angles and weir lengths. They reported the average C_d for inverted triangular weirs to be 0.61. Keshava Murthy and Giridhar [5] studied a weir of the chimney type. They showed that the linear amplitude of the chimney, compared to the inverted triangular weir, increased by more than 200%. Chatterjee et al. [6] conducted an experimental study of chimney weirs under submerged conditions. They compared the formula's performance for a submerged chimney weir with previously developed formulas for a sharp-crested weir. They concluded that the developed formula performed better than the previous methods. Chatterjee et al. [7] experimentally investigated discharge characteristics in a chimney weir under free-flow conditions. They provided a relationship for the coefficient of discharge. Hayawi et al. [8] investigated the discharge coefficient of chimney weirs at different heights of the channel floor under free and submerged conditions. The discharge coefficient in the free-flow mode increases with decreasing upstream water head, while the C_d in the submerged flow mode increases with decreasing drowning ratio. Vatankhah and Kouchakzadeh [9] used the gamma function to develop the general shape of the discharge relation for n-degree polynomial weirs and provided a solution for linear weirs. Vatankhah [10] investigated the amplitude of the linear changes of the inverted triangular weir and suggested that if the triangular cross-section is used instead of the rectangular cross-section, the error rate of deviation from the linear relation is reduced. In addition, different numerical research have been conducted on the sharp-crested weir [11-14].

Despite the previous studies, there is a few of research on using soft computing to estimate the discharge coefficient of proportional chimney weirs. The present research utilizes models such as Adaptive Neuro-Fuzzy Inference System (ANFIS), M5P, and Gaussian Process regression (GP) to evaluate the discharge coefficient.

2. Materials and Methods

2.1. Types of flow behavior in a chimney weir

In the present study, different geometric parameters of the chimney weir in the discharge rate of 0.002 to 0.009 m^3/s and water head range of 0.04 to 0.12 m above the weir crest was investigated using Daneshfaraz et al. [15] data. By placing the chimney weir in the flow path, two types of flow

behavior can be observed, and those behaviors will now be discussed.

As seen in Figure (1-a), if the water head does not exceed the inverted triangular part of the weir, the first type of behavior will occur. The discharge rate is calculated using Equation (1) [5,15].

$$Q = \frac{2}{3} C_d \sqrt{2g} L h^{3/2} - \frac{8}{15} C_d \sqrt{2g} \tan\theta \, h^{5/2} \qquad 0 \le h \le y \qquad (1)$$

Suppose the volume of water behind the weir is so high that with the addition to the inverted triangle, it also covers the area of the rectangular weir. In that case, the second behavior type will be visible, as shown in Figure (1-b). The discharge rate is calculated using Equation (2) [5,15].

$$Q = \frac{2}{3} C_d \sqrt{2g} L h^{3/2} - \frac{8}{15} C_d \sqrt{2g} \tan\theta \left(h^{5/2} - (h-y)^{5/2}\right) \qquad h > y \qquad (2)$$

where Q is the discharge, C_d is the discharge coefficient, L is the weir length, g is the gravitational acceleration, θ is the half-angle of the vertex of the triangle, y is the vertical distance between the weir crest and the first part where the weir slope changes, and h is the water head above the weir crest.

(a) (b)

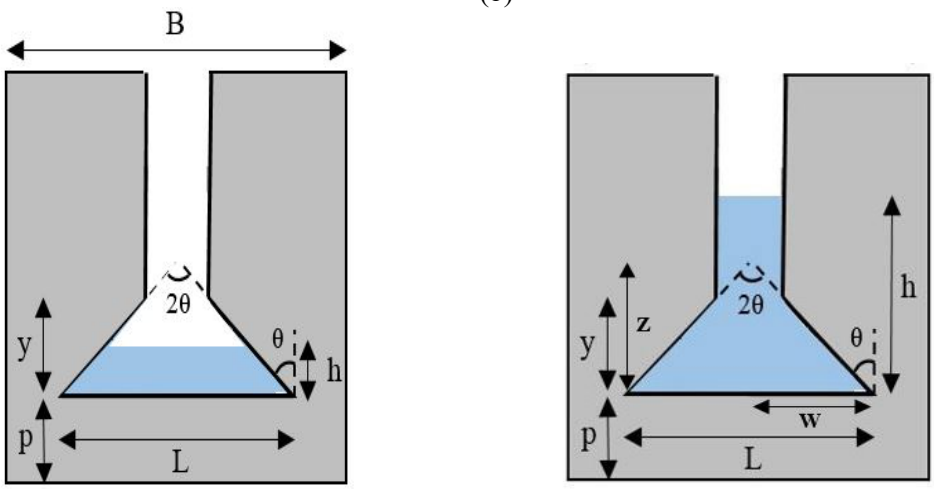

Figure 1. Schematic flow behavior in the face of chimney weir a) First type b) the Second type [15]

2.2. Applied intelligent models

Three artificial intelligence approaches were used for predicting discharge coefficients: Adaptive Neuro-Fuzzy Inference System (ANFIS), M5P, and Gaussian Process (GP). These methods will now be discussed in some detail.

2.2.1. ANFIS

According to Jang [16], an ANFIS is a hybrid network combining fuzzy and artificial neural aspects. It is equivalent to fuzzy inference systems (FIS) using distributed parameters. The fuzzy inference system (FIS) contains a set of fuzzy rules that fully describe the local behavior of the

system. Figure (2) displays a first-order Sugeno fuzzy model's structural design with two inputs and one output.

ANFIS implements and applies hybrid-learning rules to train FIS. The ANFIS approach combines the two intelligence techniques by measuring the relationship between input and target data. It uses multiple layers of feed-forward networks to handle fuzzy parameters. Multilayer feed-forward ANFIS network allows each node in the network to perform a specific function on signals received and has parameters specific to it. Essentially, it is a linear inference system corresponding to Takagi-Sugeno first-order inferences.

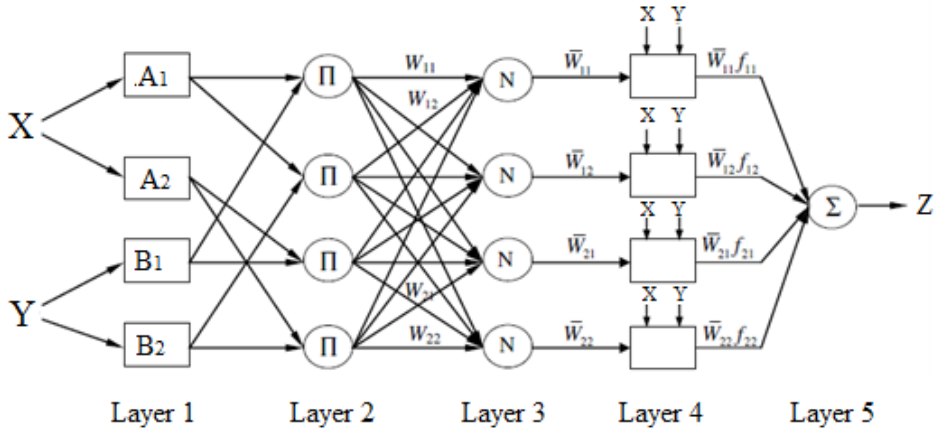

Figure 2. The schematic design of ANFIS

Layer 1 is a fuzzification layer. A set of fuzzy clusters is formulated based on membership functions. Layer 2 is known as a rule layer. The membership values calculated in the fuzzification layer are used to generate firing strengths (w_i) for the rule. The 3rd layer is the normalization layer. Normalized firing strength belonging to each node is computed in this layer. Layer 4 is a defuzzification layer. Layer 5 is the summation layer. Several important factors must be considered when developing an ANFIS model, including the training terms, membership functions, form of membership functions, and fuzzy rules. The parameters are crucial for the model's success.

2.2.2. M5P

The M5P model was created by Quinlan [17]. Model trees can handle huge datasets efficiently. They can also deal with missing data without creating any ambiguity. This tree algorithm sets a linear regression at the terminal node by classifying or dividing various data areas into multiple subspaces. It applies to each sub-location of a multivariate linear regression model. There are two stages to the creation of a model tree. A decision tree is created in the first stage using a splitting criterion. They behaved class values that reach a node as quantification of the error and the expected reduction in error because of evaluating each attribute at that node are calculated as branching criteria for the M5P tree model algorithm [17]. The separation criteria predict the standard deviations of class values extending to nodes, permitting the basic tree model to be generated. The method uses the standard deviation to measure the predicted error at the terminal node.

$$SDR = sd(N) - \frac{\sum_{i=1}^{x}|N_i|}{|N|} * sd(N) \quad (3)$$

In Equation (3), N is the number of samples, and sd represents the standard deviation.

2.2.3. GP

The GP regression is based on the notion that adjoining observations should transfer information about each other [18]. The GP is a method of describing a prior explicitly across function space. The GP can define a prior probability over a latent function. The GP model design involves a kernel function. Many kernels are discussed in the literature [19-21]. Here, the Polynomial and Radial Basis Function (RBF) kernel are used.

2.3. Statistical indicators

The statistical indicators of CC, MAE, RMSE, NSE, and SI were used to investigate the accuracy of models [22-23].

$$CC = \frac{\sum_{i=1}^{N}(R_i-\bar{R})(Q_i-\bar{Q})}{\sqrt{\sum_{i=1}^{N}(R_i-\bar{R})^2\sum_{i=1}^{N}(Q_i-\bar{Q})^2}} \qquad -1 \le CC \le 1 \quad (4)$$

$$MAE = \frac{1}{N}\sum_{i=1}^{N}|R_i - Q_i| \quad (5)$$

$$RMSE = \sqrt{\frac{1}{N}\sum_{i=1}^{N}(R_i - Q_i)^2} \quad (6)$$

$$NSE = 1 - \left(\frac{\sum_{i=1}^{N}(R_i-Q_i)^2}{\sum_{i=1}^{N}(Q_i-\bar{Q})^2}\right) \qquad -\infty \le NS \le 1 \quad (7)$$

$$SI = \frac{\sqrt{\frac{1}{N}\sum_{i=1}^{N}(R_i-Q_i)^2}}{\overline{Q}} \quad (8)$$

where CC is the Correlation Coefficient, RMSE is the Root Mean Square Error, MAE is the Mean Absolute Error, NSE is the Nash Sutcliffe Efficiency, and SI is the Scattering Index. The Q and $\bar{Q}$ represent the actual values and the mean observed values, respectively, R is the predicted values, and N is the total of observations [24].

2.4. Implementation of machine learning-based models

The models were trained and tested for predicting C_d based on four input variables: h/p, y/p, L/p, and w/z. Machine learning models, including ANFIS, M5P, and GP, were established using Matlab and Weka software.

3. Results and Discussion

Here, 110 observations were collected; including measurements of h/p, y/p, L/p, w/z, and C_d. Table (1) reveals that h/p has a higher negative correlation (-0.6775) with C_d.

Out of 110 observations, 77 were chosen for the training phase and the rest for the testing phase [25]. h/p, y/p, L/p and w/z were independent variables, whereas C_d was dependent. Table (2) shows the model components' descriptive data statistics for training and testing data sets.

Table 1. The results of the correlation matrix

Variables (-)	*h*/*p*	*y*/*p*	*L*/p	*w*/*z*	C_d
h/*p*	1				
y/*p*	0.059551	1			
L/*p*	0.213261	0.279243	1		
w/*z*	7.56E-13	-0.93496	6.73E-17	1	
C_d	-0.67755	-0.38013	0.220204	0.456796	1

Table 2. The statistics of model

Statics	*h*/*p*	*y*/*p*	*L*/*p*	*w*/*z*	C_d
			Training		
Mean	1.392393	0.910631	2.736549	1.144406	0.664879
Median	1.428571	0.828571	2.528571	1.079902	0.662973
Standard Deviation	0.50138	0.258106	0.212078	0.309522	0.010691
Kurtosis	-1.13825	-0.96737	-2.05333	-1.33073	0.313114
Skewness	0.064846	0.374496	0.026495	0.266493	0.645531
Minimum	0.571429	0.559118	2.528571	0.753554	0.646613
Maximum	2.333333	1.385309	2.95	1.600335	0.697535
Confidence Level (95.0%)	0.113799	0.058583	0.048136	0.070253	0.002427
			Testing		
Mean	1.393939	0.93966	2.745671	1.103879	0.665375
Median	1.333333	0.966667	2.95	1.079902	0.664821
Standard Deviation	0.520215	0.248274	0.213883	0.292291	0.010301
Kurtosis	-0.90186	-1.04983	-2.12903	-1.03808	-0.76897
Skewness	0.164531	0.213658	-0.06356	0.439045	0.177143
Minimum	0.571429	0.559118	2.528571	0.753554	0.648
Maximum	2.333333	1.385309	2.95	1.600335	0.684757
Confidence Level (95.0%)	0.18446	0.088034	0.07584	0.103642	0.003653

The triangular, trapezoidal, generalized bell shapes, and Gaussian shapes of membership functions (MFs) were chosen to predict C_d. The optimum number of MFS are 4, 3, 4, and 4 for input variables. In Table (3), the performance of the triangular MF–based ANFIS (ANFIS-ti) model is better than other ANFIS-based models for predicting the C_d. The results of CC, MAE, RMSE, SI, and NSE for the training phase are 0.9652, 0.0018, 0.0028, 0.0042 and 0.9317, respectively. In addition, the results for the test phase are 0.9505, 0.0025, 0.0032, 0.0048 and 0.9, respectively. Figure (3) represents that the predicted values using ANFIS-based models is closer to the agreement line. Table (3) and Figure (6) confirm that the predictive performance of the ANFIS-ti-based model is better than other ANFIS-based models in predicting C_d.

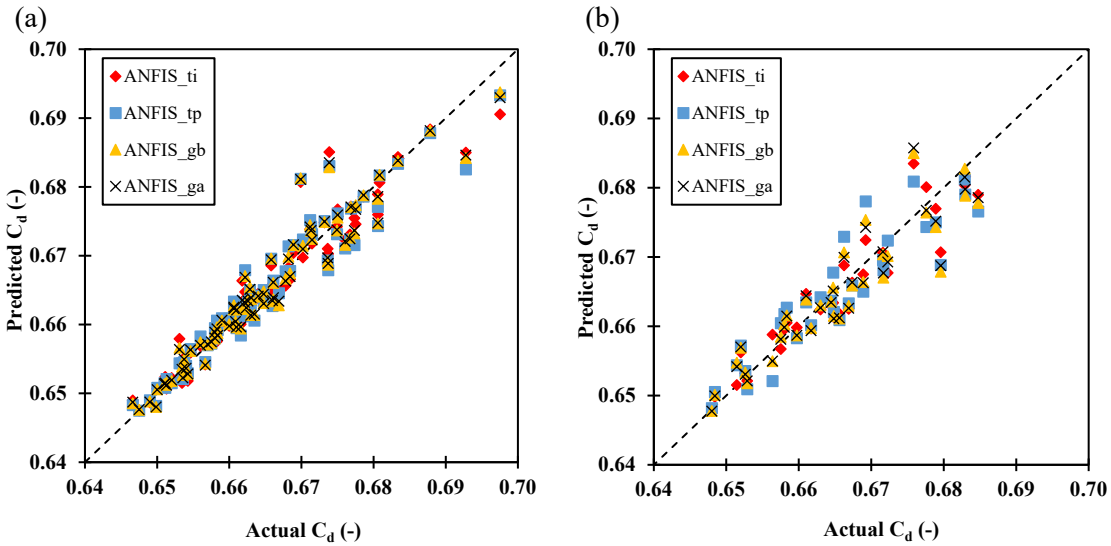

Figure 3. Actual against predicted C_d in ANFIS-based models a) Train phase, b) Test phase

Table 3. Performance of all applied models

Models	CC	MAE	RMSE	NSE	SI
			Training		
ANFIS-ti	0.9652	0.0018	0.0028	0.9317	0.0042
ANFIS-tp	0.9571	0.0021	0.0031	0.9161	0.0046
ANFIS-gb	0.9639	0.0019	0.0028	0.9292	0.0043
ANFIS-ga	0.9649	0.0019	0.0028	0.9311	0.0042
M5P	0.9533	0.0023	0.0033	0.9063	0.0049
GP-poly	0.9532	0.0024	0.0032	0.9085	0.0048
GP-rbf	0.9703	0.0018	0.0026	0.9415	0.0039
			Testing		
ANFIS-ti	0.9505	0.0025	0.0032	0.9001	0.0048
ANFIS-tp	0.9123	0.0034	0.0042	0.8300	0.0063
ANFIS-gb	0.9220	0.0030	0.0040	0.8467	0.0060
ANFIS-ga	0.9293	0.0029	0.0038	0.8602	0.0057
M5P	0.9568	0.0024	0.0032	0.9022	0.0048
GP-poly	0.9472	0.0026	0.0033	0.8925	0.0050
GP-rbf	0.9344	0.0026	0.0037	0.8700	0.0055

Implementation of the M5P-based model uses an iterative process. Many trials were performed to attain the values of optimum user-defined parameters. The optimum values of user-defined parameters are 4. Here, an unpruned model was developed for predicting C_d. In Table (3), the performance of the M5P model is desirable for predicting the C_d. The CC, MAE, RMSE, SI, and NSE for the training phase are 0.9533, 0.0023, 0.0033, 0.0049 and 0.9063, respectively. The value of these parameters for the test phase are 0.9568, 0.0024, 0.0032, 0.0048 and 0.9022, respectively. Figure (4) shows the results of the actual and predicted amounts in the M5P-based model.

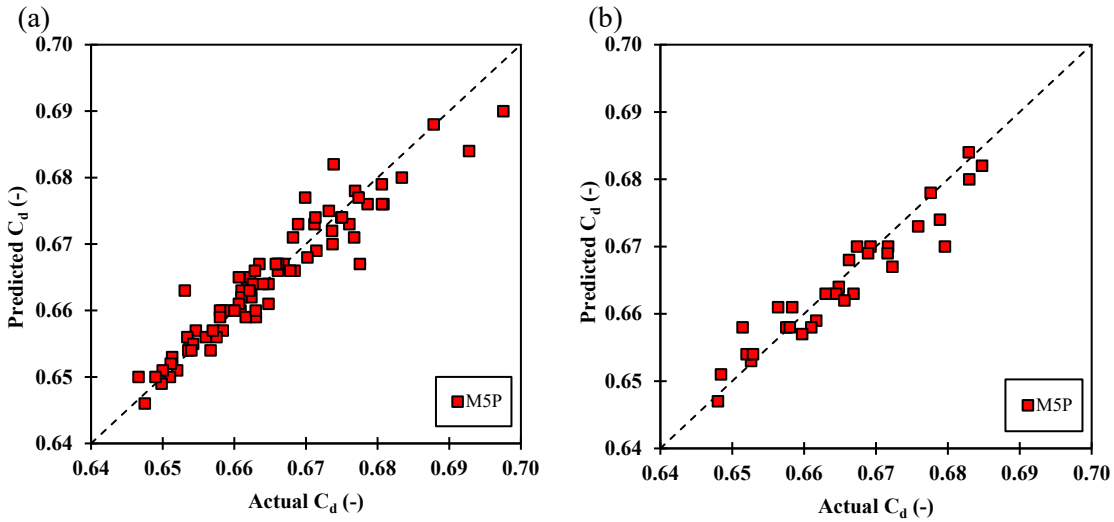

Figure 4. Actual against predicted C_d in M5P-based model a) Train phase, b) Test phase

Implementation of GP-based models is iterative, similar to the M5P model. Many trials were carried out to attain the values of optimum user-defined parameters. Here, the polynomial and RBF were used to predict the C_d. For the polynomial (GP-polynomial), the optimal user-defined parameters are 0.01 for noise and d=3. In addition for the RBF (GP-RBF), the value of noise is kept constant (0.01) for fair comparison among both developed models and γ=1. As seen from Table (3), the performance of the GP-polynomial-based model is better than the GP-RBF-based model for predicting C_d. In the train phase, the results of the CC, MAE, RMSE, SI, and NSE statistical indicator are 0.9532, 0.0024, 0.0032, 0.0048, and 0.9058. For the test phase, the results are 0.9472, 0.0026, 0.0033, 0.005 and 0.9925, respectively. Figure (5) shows that the performance of the GP-polynomial-based model is better than GP-RBF-based models in predicting C_d.

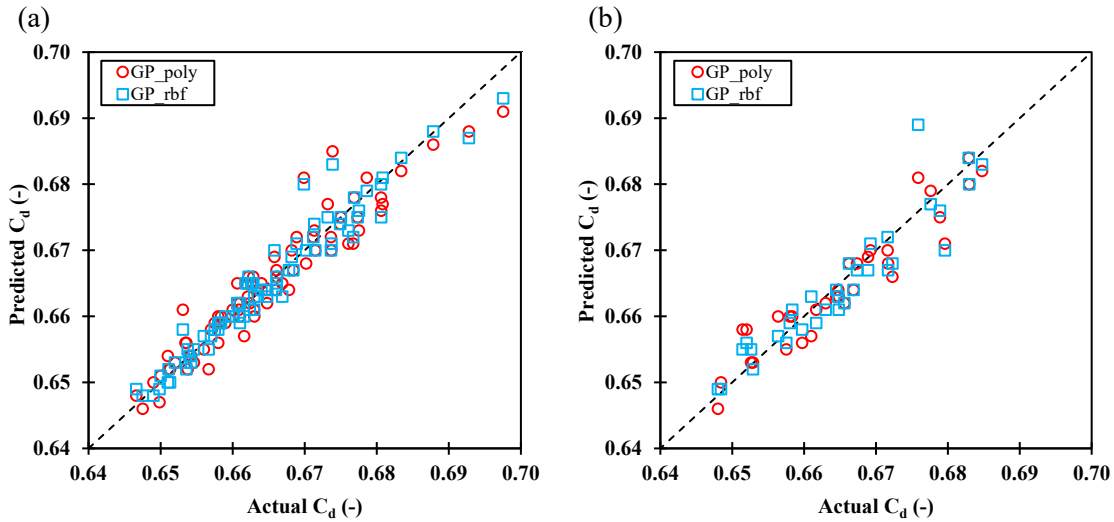

Figure 5. Actual against predicted C_d in GP-based models a) Train phase, b) Test phase

A comparison of the ANFIS, M5P, and GP models shows that the results in M5P model are more favorable than other models. Compared to ANFIS and GP-based models, the triangular MFS-based ANFIS model results are good than the GP and ANFIS-based models. Figure (6) shows the values of C_d in ANFIS, M5P, and GP-based models. The results showed that the values of the predicted C_d using M5P model are the best. Figure (6-c) shows that predicted values using M5P-based models match actual values with minimum deviation (Figure 6-d).

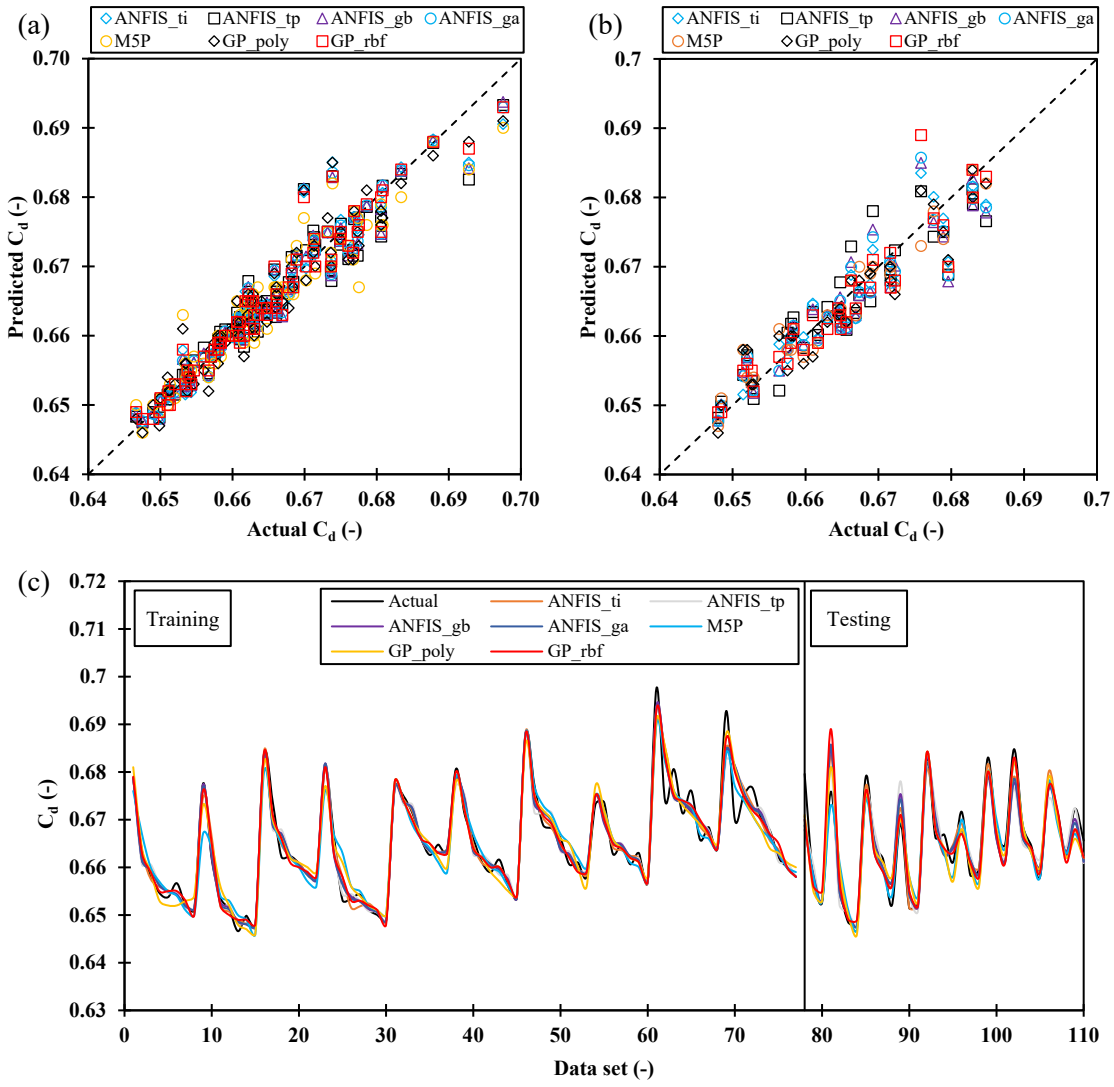

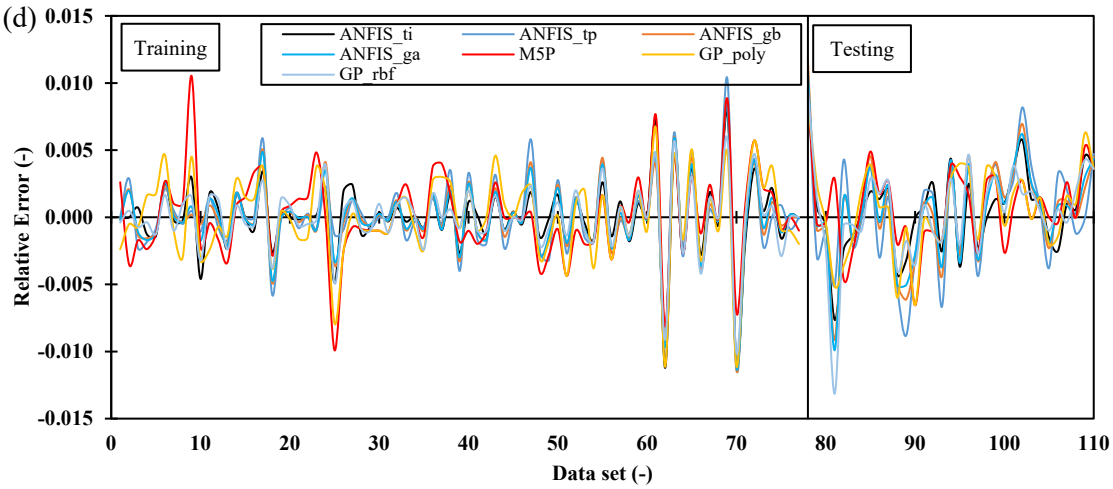

Figure 6. Actual against predicted values of C_d in various machine learning-based models a) Train phase, b) Test phase, c) Performance, d) RE

To investigate the inconsistency of the mass flow rate prediction with the actual values, the 25%, 50%, and 75% quartile values of the actual and predicted C_d values are listed in Table (4). The box plot diagram and Taylor diagram were used to examine the models' accuracy (Figure 7 and 8). Figure (7 and 8), display all variations between the actual and predicted values.

When both Table (4) and Figure (7) are examined, the min, the max, 25% quartile value (Q_1), 75% quartile value (Q_3), and the median value (Q_2) for M5P and the actual values are very close. When comparing the actual data and the predicted values of the M5P-based model, the width of the higher and lower boxes is almost the same (Figure 7-a and b).

Table 4. Quantitative statistics of actual data and predicted values for all models

Statistic	Actual	ANFIS-ti	ANFIS-tp	ANFIS-gb	ANFIS-ga	M5P	GP-poly	GP-rbf
	Training							
Minimum	0.6466	0.6475	0.6475	0.6476	0.6477	0.6460	0.6460	0.6480
Maximum	0.6975	0.6905	0.6933	0.6937	0.6930	0.6900	0.6910	0.6930
1st Quartile	0.6575	0.6576	0.6580	0.6574	0.6575	0.6570	0.6580	0.6580
Median	0.6630	0.6637	0.6633	0.6631	0.6634	0.6640	0.6640	0.6640
3rd Quartile	0.6715	0.6723	0.6724	0.6724	0.6723	0.6720	0.6720	0.6720
IQR	0.0140	0.0147	0.0144	0.0150	0.0148	0.0150	0.0140	0.0140
	Testing							
Minimum	0.6480	0.6478	0.6482	0.6478	0.6478	0.6470	0.6460	0.6490
Maximum	0.6848	0.6835	0.6812	0.6850	0.6858	0.6840	0.6840	0.6890
1st Quartile	0.6580	0.6595	0.6602	0.6587	0.6587	0.6580	0.6580	0.6580
Median	0.6648	0.6630	0.6637	0.6636	0.6634	0.6630	0.6630	0.6630
3rd Quartile	0.6717	0.6706	0.6724	0.6704	0.6700	0.6700	0.6700	0.6700
IQR	0.0137	0.0111	0.0122	0.0117	0.0113	0.0120	0.0120	0.0120

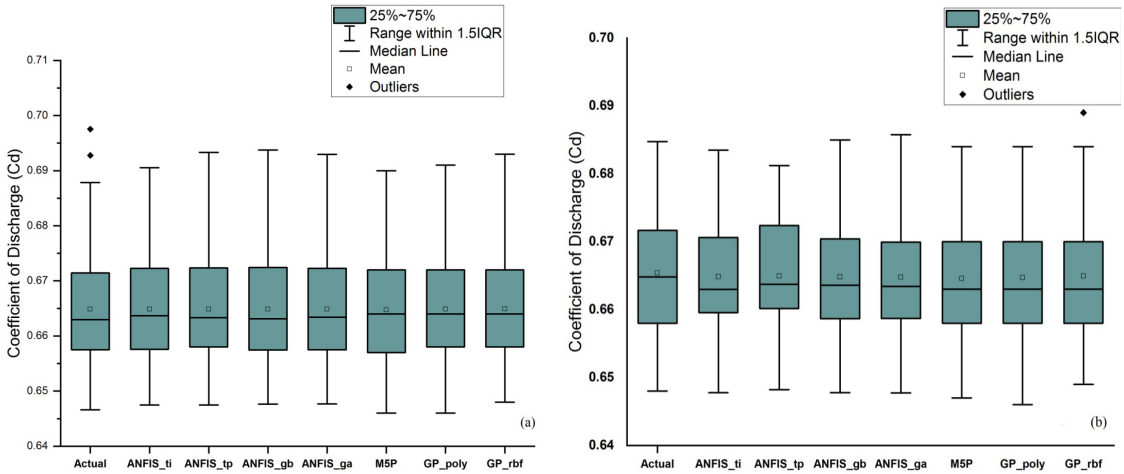

Figure 7. Box plot of relative errors using all applied models a) Train phase, b) Test phase

According to Taylor diagram, the best performing model is closer to the actual point. Taylor diagram indicates that the M5P-based model has the highest accuracy in the testing phase for predicting C_d (Figure 8).

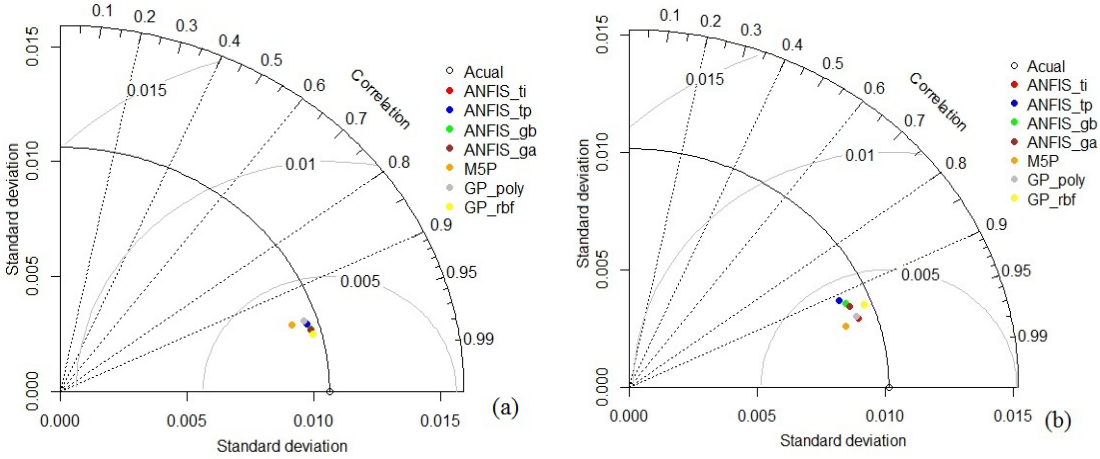

Figure 8. Taylor diagram a) Training, b) Testing

3. Conclusions

In the present research, chimney weirs were tested with apex angles of 74˚, 84˚, 94.4˚, 106˚, and 116˚ at crest heights of 0.06 and 0.07 m. The discharge and head above the crest for the modeled weirs were in the range of 0.002 to 0.009 m^3/s, and 0.04 to 0.12 m, respectively. The various machine learning-based models Adaptive Neuro-Fuzzy Inference System (ANFIS), M5P, and Gaussian Process (GP) were used to predict the C_d. 5 various goodness-of-fit parameters and various graphical presentations were used to evaluate the performance of the developed machine learning models. It was found that M5P based model was superior to other models in predicting C_d. The results showed that the ANFIS-ti model was better than GP and other MF-based ANFIS models. On the other hand, the performance of the Trapezoidal MF-based ANFIS (ANFIS-tp) model was the worst among all applied models. Based on the sensitivity results using M5P models, h/p is followed by L/p.

References

1. Keshava Murthy K, Pillai K.G, (1978). Design of constant accuracy linear proportional weir. Journal of the Hydraulics Division, 104: 527-541.
2. Bos M.G, (1998). Discharge measurement structures. International institute for land reclamation and improvement (ILRI). Publication No. 20, Wageningen, The Netherlands.
3. Ramamurthy A.S, Subramanya K, Pani B.S, (1977). Quadrant-plate weirs. Journal of Hydraulic Engineering Division, 103: 1431-1441.
4. Keshava Murty K, Giridhar D.P, (1989). Inverted v-notch: practical proportional weir. Journal of Irrigation and Drainage Engineering, 115: 1035-1050.
5. Keshava Murthy K, Giridhar D.P, (1990). Improved inverted v-notch or chimney weir. Journal of Irrigation and Drainage Engineering, 116: 374-386.
6. Chatterjee C, Singh R, Kar S.K, Panda S.N, Vohra S.L, (1998). Flow characteristics of chimney weir under submergence. Journal of Irrigation and Drainage Engineering, 124: 96-101.
7. Chatterjee C, Singh R, Kar S.K, (2002). Discharge characteristics of chimney weir under free-flow conditions. Journal of Irrigation and Drainage Engineering, 128(3): 175-179.
8. AM Hayawi H, AG Yahya A, AM Hayawi G, (2005). COEFFICIENT OF DISCHARGE OF CHIMNEY WEIR UNDER FREE AND SUBMERGED FLOW CONDITIONS. Al-Rafidain Engineering Journal (AREJ), 13(1): 62-69.
9. Vatankhah A.R, Kouchakzadeh S, (2009). Discussion of head-discharge equation for sharp-crested polynomial weir, by Baddour, R.E. Journal of Irrigation and Drainage Engineering, 135: 393-395.
10. Vatankhah A.R, (2012). Head-discharge equation for sharp-crested weir with piecewise-linear sides. Journal of Irrigation and Drainage Engineering, 138: 1011-1018.
11. Bilhan O, Cihan A, Emiroglu M.E, Miller C.J, (2018). Experimental and CFD analysis of circular labyrinth weirs. Journal of Irrigation and Drainage Engineering, 144(6): 04018007.
12. Ghaderi A, Dasineh M, Abbasi S, Abraham J, (2019). Investigation of trapezoidal sharp-crested side weir discharge coefficients under subcritical flow regimes using CFD. Applied Water Science, 10: 1-12.
13. Norouzi R, Daneshfaraz R, Ghaderi A, (2019). Investigation of discharge coefficient of trapezoidal labyrinth weirs using artificial neural networks and support vector machines. Applied Water Science, 9: 148.
14. Norouzi R, Arvanaghi H, Salmasi F, Farsadizadeh D, Ghorbani M.A, (2020). A new approach for oblique weir discharge coefficient prediction based on hybrid inclusive multiple model. Flow Measurement and Instrumentation, https://doi.org/10.1016/j.flowmeasinst.2020.101810
15. Daneshfaraz R, Norouzi R, Abbaszadeh H, (2023). Effect of geometric shapes of chimney weir on discharge coefficient. Journal of Applied Water Engineering and Research, DOI: 10.1080/23249676.2023.2192977.
16. Jang J.S, (1993). ANFIS: adaptive-network-based fuzzy inference system. IEEE transactions on systems, man, and cybernetics, 23: 665-685.
17. Quinlan J.R, (1992). Learning with continuous classes. In 5th Australian joint conference on artificial intelligence, 92: 343-348.
18. Williams C.K, Rasmussen C.E, Gaussian processes for machine learning (Vol. 2, No. 3, p. 4). Cambridge, MA: MIT press, 2006.

19. Xing W, Shah A.A, Nair P.B, (2015). Reduced dimensional Gaussian process emulators of parametrized partial differential equations based on Isomap. Proceedings of the Royal Society A: Mathematical, Physical and Engineering Sciences, 471(2174): 20140697.
20. Sihag P, Tiwari N.K, Ranjan S, (2017). Modelling of infiltration of sandy soil using Gaussian process regression. Modeling Earth Systems and Environment, 3: 1091-1100.
21. Kumar D, Roshni T, Singh A, Jha M.K, Samui P, (2020). Predicting groundwater depth fluctuations using deep learning, extreme learning machine and Gaussian process: a comparative study. Earth Science Informatics, 13: 1237-1250.
22. Daneshfaraz R, Norouzi R, Abbaszadeh H, Azamathulla H.M, (2022). Theoretical and experimental analysis of applicability of sill with different widths on the gate discharge coefficients. Water Supply, 22(10): 7767-7781. https://doi.org/10.2166/ws.2022.354
23. Abbaszadeh H, Daneshfaraz R, Norouzi R, (2023). Experimental Investigation of Hydraulic Jump Parameters in Sill Application Mode with Various Synthesis. Journal of Hydraulic Structures, 9(1): 18-42. doi: 10.22055/jhs.2023.43208.1245.
24. Daneshfaraz R, Norouzi R, Abbaszadeh H, Kuriqi A, Di Francesco S, (2022). Influence of Sill on the Hydraulic Regime in Sluice Gates: An Experimental and Numerical Analysis. Fluids, 7(7): 244. https://doi.org/10.3390/fluids7070244.
25. Hassanzadeh Y, Abbaszadeh, H. (2023). Investigating Discharge Coefficient of Slide Gate-Sill Combination Using Expert Soft Computing Models. Journal of Hydraulic Structures, 9(1): 63-80. doi: 10.22055/jhs.2023.43683.1251